A metal-dielectric antenna for terahertz near-field imaging

N. Klein,[a] P. Lahl, and U. Poppe
Institut fur Schichlen und Grenzflachen, Forschungszentrum Jülich, Gesellschaft Mit Beschränkter Haftung (GmbH), Center of Nanoelectronics and Information Technology (CNI), D 52425, Jülich, Germany

F. Kadlec and P. Kužel
Institute of Physics, Academy of Sciences of the Czech Republic, Na Slovance 2, 182 21 Prague 8, Czech Republic

We present an antenna-based approach to near-field imaging and spectroscopy, which can be used for both continuous-wave and pulsed broadband electromagnetic radiations from microwave to terahertz frequencies. Our near-field antenna consists of a rectangular-shaped block of low-loss dielectric material sharpened to a pyramidal tip which is partially metallized and terminated by a micron-sized plane facet. At this facet the entire energy of the incident wave is concentrated as a very high but strongly localized electric field, which can be used as a sensitive near-field microprobe for electromagnetic radiation. Currently, experiments in reflection geometry with pulsed terahertz radiation and continuous-wave radiation near 80 GHz reveal a frequency-independent spatial resolution of about 20 μm corresponding to $\lambda/200$ at 80 GHz, which is only limited by the size of the facet terminating the tip. © *2005 American Institute of Physics*. [DOI: 10.1063/1.1978972]

I. INTRODUCTION

Terahertz imaging techniques have gained increasing recognition as a promising method with various applications,[1] e.g., for dermatological and oral imagings,[2] and for various tasks related to material inspection.[3] Usually, a beam of pulsed terahertz radiation is scanned over the sample to be imaged, and the analysis of the transmitted or reflected pulse yields information on the sample properties.[4,5] Another technique relies on a space-resolved analysis of the output beam such that single-shot images[6,7] or even three-dimensional tomographic data[8] can be obtained. However, since the wavelength of terahertz radiation is on the order of 300 μm, the diffraction-limited spatial resolution is insufficient for many possible applications. Recently, various approaches to terahertz near-field imaging have been suggested, such as subwavelength size apertures[9,10] and scattering from a metallic needle positioned close to the surface to be imaged.[11–13] The drawback of such methods is the relatively small portion of pulse energy available as a localized field probe enabling subwavelength resolution. In contrast, near-field methods at microwave frequencies rely on tapered metal transmission lines where subwavelength resolution can be easily attained.[14] However, metal transmission lines such as coaxial lines or coplanar tips are very lossy and difficult to machine for the frequency range above 50–100 GHz. Golosovsky and Davidov developed a millimeter-wave near-field microscope based on a resonant slot antenna either for a metallic waveguide[15] or for a metal-coated dielectric resonator.[16] Due to the resonant properties of the slot, this approach is limited to a fixed frequency. For the optical frequency range, subwavelength imaging by scanning near-field optical microscopy (SNOM) often relies on metallized glass tips, and therefore represents a subwavelength aperture method, which is substantially different from our approach.[17,18]

II. DESCRIPTION OF OUR TERAHERTZ NEAR-FIELD ANTENNA

Here, we present an approach for converting a guided gigahertz wave or a free-propagating tetrahertz wave into a quasistatic capacitor field acting as a confined field probe, which provides a subwavelength resolution without significant losses and dispersion. We show that the currently achieved spatial resolution of 25 μm is limited by the fabrication technique used for our near-field antenna (NFA). This indicates that, in the future, micron or even submicron resolution should be feasible by our approach.

Figure 1 shows a schematic drawing of our NFA. A block of a low-loss dielectric material is machined. In our case, we have cut the needle bars of about 13-mm length and a cross section of 2×1 mm^2 from a wafer of highly resistive ($\rho \approx 3$ kΩ cm) silicon. According to Fig. 1(a), a pyramidal-shaped tip of about 3-mm length is created at one end of the bar by mechanical polishing. The pyramidal tip is terminated by a flat end facet of micrometer size, which ideally has the same aspect ratio as the bar cross section. As the most important step enabling subwavelength resolution, two opposite side facets of the pyramid need to be coated with highly conducting metal layers being sufficiently thick in terms of the skin depth. Since the facets to be coated and those to remain uncoated are at 90° angle with respect to each other, we employed ultrahigh-vacuum electron-beam evaporation as a highly directional metal deposition technique. The coating consisted of a 10-nm titanium adhesive layer, 1 μm of silver, and 30 nm of gold as a protection layer. By carefully aligning the needles in the vacuum chamber, such that the facet to be coated is facing the flight direction of the atoms,

---

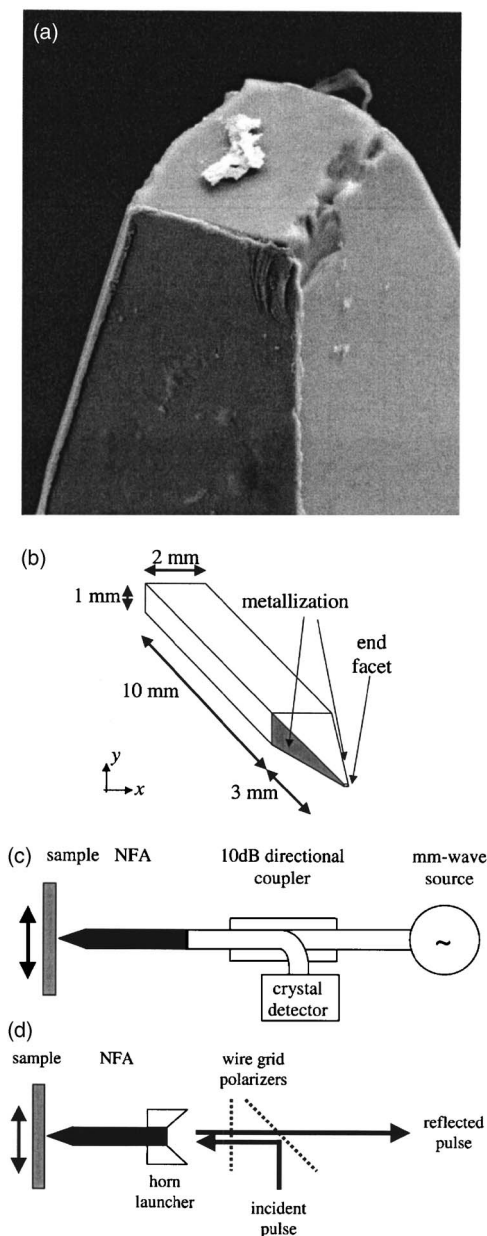[a]Author to whom correspondence should be addressed; electronic mail: n.klein@fz-juelich.de

FIG. 1. (a) SEM picture of the tip, (b) scheme of the near-field antenna, and experimental setups for (c) continuous-wave monochromatic and (d) pulsed broadband measurements. The particle on the flat output facet in Fig. 1(a) is dust.

the required partial coating was realized without any lithography, as shown by the scanning electron microscopy (SEM) picture of the tip [Fig. 1(b)]. According to Fig. 1(b) the end facet of the tip that we used in our experiments was found to have a rectangular shape of 30×40 μm^2.

Figures 1(c) and 1(d) indicate how the NFA is arranged for imaging the reflected signal. For measurements at discrete frequencies in the millimeter-wave range [Fig. 1(c)], the NFA of 2×1 mm^2 cross section is attached to the open end of a metal waveguide of the same cross section. The reflected signal is measured by a standard setup utilizing a directional coupler and a detector diode. In Fig. 1(d) a quasioptical arrangement is displayed which is particularly suited for pulsed terahertz radiation. Our time-domain terahertz setup employs amplified pulses (pulse length of 50 fs,

central wavelength of 810 nm, and repetition rate of 1 kHz) for the terahertz generation (spectral range of 0.1–2.5 THz) and electro-optic sampling detection by 1-mm ZnTe crystals.[19] About 50% of the power of the incoming terahertz beam is directed to the 2×1-mm^2 input facet (flat end) of the NFA via a wire grid polarizer, which is arranged at an angle of 45° with respect to the propagation direction of the beam. Another wire grid polarizer ensures that the polarization of the wave inside the NFA is perpendicular to the metallized planes of the pyramidal tip. In order to improve the input coupling to the NFA, the antenna is mounted inside a metallic horn launcher with a square cross section of 4×4 mm^2, which is slightly larger than the focal waist of the terahertz beam at the entry.

Figure 2(a) shows the measured amplitude of the reflected signal in continuous-wave experiments as a function of frequency between 74 and 92 GHz and the results of a numerical field simulation performed using the CST Microwave Studio software.[20] The dips with a frequency separation of about 3 GHz correspond to standing waves inside the NFA due to reflections at the end facet of the tip and the opposite flat end of the bar. The calculated distribution of the electric field at a dip frequency displayed in Fig. 2(b) clearly illustrates the operation principle of the NFA: at the input facet, the incoming wave is primarily converted into the fundamental mode of a dielectric waveguide. For lower frequencies, down to dc, a coaxial cable could be attached to the metallized pads by bonding if the metal coating is extended over the straight sections of the NFA (not shown in the figures).

Upon entering the pyramidal-shaped tip, the dielectric waveguide mode is gradually converted into a stripline mode where the electric field is confined between the two metallization pads. It is worth to note that for a pyramidal-shaped tip the aspect ratio is maintained throughout the tip resulting in constant wave impedance along the tip, such that the wave is not reflected before it reaches the micrometer-sized termination (end facet). Figure 2(c) indicates the fringe field at the tip termination, which is spatially confined on the scale of the width of the facet. Note that the amplitude of the electric field at the tip is very high, and corresponds to a constant voltage drop between the metallized pads.

The insert of Fig. 2(a) indicates the influence of a metal plate, a sapphire substrate, and a wet sheet of paper brought into a direct contact with the end facet. The significant changes of the reflected amplitude for the different materials are clear fingerprints of the interaction of the fringe field with a matter in its close vicinity. This allows the probing of a possible contrast in the sample dielectric and conductive properties with a spatial resolution determined by the size of the end facet. It is worth to emphasize that the effect of the wet paper on the amplitude of the reflected signal is very strong. This shows that the method is well suited for investigation of tissue samples. As shown by the analysis of the field simulation, multiple dips apparent both in the simulation and in the experimental data correspond to higher-order dielectric waveguide modes in the straight section of the NFA. A detailed analysis, which should allow one to determine the real and imaginary parts of the dielectric function
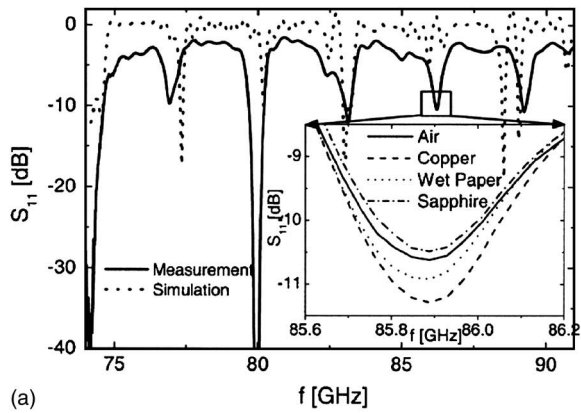
(a)
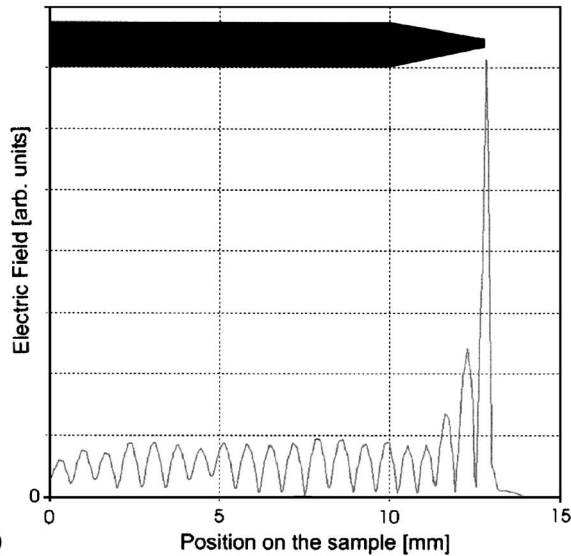
(b)
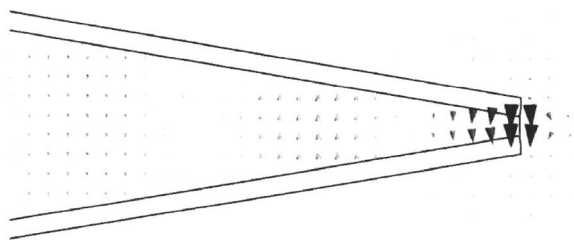
(c)

FIG. 2. (a) Measured amplitude of the normalized reflected signal (two-port *S*-parameter S_{11}) for monochromatic radiation at around 80 GHz measured by using the setup shown in Fig. 1(b) in comparison to a numerical field simulation. Both curves exhibit standing-wave resonances in the NFA. The resonance *Q* values reach up to 2000 in the experiment depending on the coupling. Insert: modification of such a resonance by various materials placed in front of the tip. [(b) and (c)] Simulated electric field for a frequency corresponding to a resonance peak position. The distance between the metallized pads at the tip termination is 50 μm. (b) shows the electric-field magnitude at the axis of the NFA as function of position along the length of the NFA and demonstrates the standing-wave pattern and the field enhancement in front of the needle. From the field simulation the electric field at the end facet of the tip was found to be a factor of 8.6 higher than in the straight part of the NFA. (c) Simulated distribution of the electric field in the NFA at a position near the tip demonstrating the focusing effect.

of the sample independently, by monitoring the amplitude and frequency changes of each standing-wave resonance, still needs to be performed. Due to the high density of equally separated resonances and the broadband properties of the antenna, this method is generally suited to yield spectroscopic information on the sample properties. As an alterna-
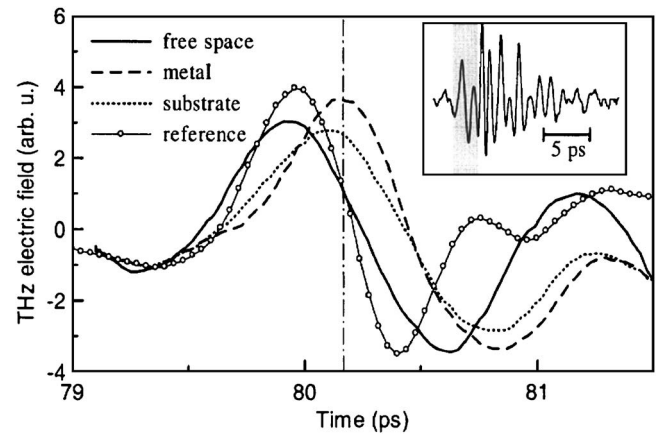

FIG. 3. Waveforms corresponding to first oscillations of the terahertz pulse reflected from the tip obtained in a contact mode with several media: air (free space), metal, and lanthanum aluminate substrate. In comparison, we show as a reference waveform the signal reflected directly from the input facet of the needle (vertically scaled by a factor of 0.3 and horizontally shifted by 280 ps for this plot). Inset: entire waveform reflected at the tip obtained for the free space mode; the gray part corresponds to the main plot.

tive approach, broadband-matched input coupling may by achieved by cutting the input facet of the NFA at the corresponding Brewster angle of the NFA dielectric material.

The insert of Fig. 3 shows the shape of the terahertz pulse reflected from the end facet of the NFA in comparison with the reference pulse reflected directly from the input facet. The integrated intensity of this pulse was found to be about 10% of that of the input one-and-half-cycled pulse. The pulse reflected from the input facet of the NFA (not displayed) is displaced by about 280 ps, corresponding to the optical length of the NFA. According to Fig. 3, the shape of the first oscillation of the pulse reflected from the tip was found to be strongly affected by a metal film or a dielectric substrate brought into a direct contact with the end facet. We assume that this part of the peak corresponds to the fraction of electromagnetic energy transported by the fundamental mode of the dielectric waveguide, where the field distribution is similar to the one shown in Fig. 2(b). The Fourier analysis of the pulses (not shown) indicates that the spectral weight of the pulses reflected at the NFA tip is redshifted compared to the reference pulse; qualitatively, this redshift seems to increase with decreasing impedance of the probed medium. However, in order to perform spectroscopic measurements using our method, frequency-dependent radiation losses and dispersion inside the tip should be more thoroughly understood. The additional oscillations visible in the insert of Fig. 3 are either caused by higher-order dielectric waveguide modes or by waveguide dispersion. To distinguish between those two mechanisms, experiments with NFAs of different length and cross section and with improved input coupling are in progress.

III. INVESTIGATION OF SPATIAL RESOLUTION

In order to test the spatial resolution of our NFA, we placed an *xy* scanning table in front of the tip within our terahertz time-domain setup. As a sample we employed a lanthanum aluminate substrate with a patterned metal film
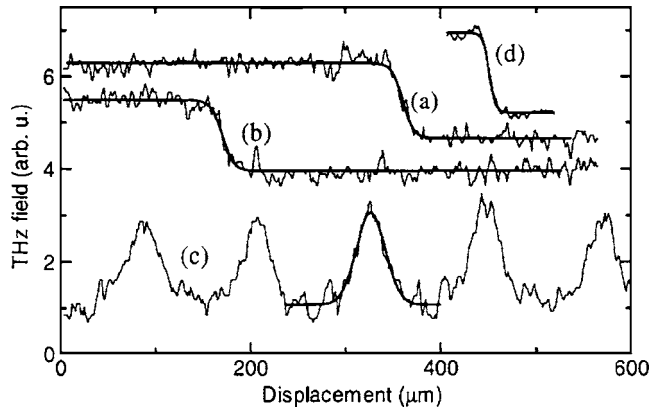
FIG. 4. Examples of *x* and *y* scans of the sample (metal stripes deposited on a lanthanum aluminate substrate). [(a)–(c)] Pulsed broadband setup [following Fig. 1(d)]; scans were performed at a fixed delay time of 80.17 ps (dash-dotted line in Fig. 3): (a) *y* scan and (b) *x* scan across a metal stripe edge; (c) *x* scan across a pattern of 60-μm metal stripes separated by 60 μm. (d) Continuous-wave monochromatic setup at 80 GHz [following Fig. 1(c)]; *x* scan over a metal edge. The vertical offsets of the data were introduced for clarity.

FIG. 5. Illustration of the ability to perform two-dimensional scans: image at 80 GHz of a 1-mm-wide metal stripe and an array of 30-μm-wide stripes (lower values of intensity) being separated by gaps of 30 μm. The stripes have been prepared by photolithography of a metal film on a lanthanum aluminate substrate. The scanning speed was 40 μm/s; the separation between two adjacent scanned lines was 10 μm.

attached to the scanning table by soft springs. The scanning experiments were performed at a speed of 10 μm/s, in a contact mode such that the tip touches the sample. According to the results depicted in Fig. 3, we recorded the signal at a delay time of 80.17 ps, where the contrast between lanthanum aluminate (permittivity=23) and metal is at maximum. Figure 4 shows the signal as a function of the sample position upon scanning over the edges of a patterned metallic film. The scans were performed both in *x* direction [corresponding to the intersection of the planes of nonmetallized side facets of the tip, see Fig. 1(a)] and *y* direction (perpendicular to *x*). The data corresponding to the edge region were fitted by a sigmoidal function which revealed a spatial resolution (width of the 90%–10% level drop) of about 27 and 25 μm for the scanning directions *x* and *y*, respectively. This resolution is slightly better than what would correspond to the top facet dimensions. We attribute this to the fact that in the contact mode a high-frequency short between the two metal facets is generated when the tip touches the metal with its physical edge. We checked that the resolution is lower when the metal surface is further away from the end facet. For this purpose we scanned over the edge of a metal strip separated from the tip termination by a 50-μm-thick plastic foil. In this case the spatial resolution was found to be 50 μm.

Curve (c) in Fig. 4 shows the results of a one-dimensional *x* scan across an array of 60-μm metal stripes separated by 60 μm on a lanthanum aluminate substrate. In this case the fit of the peaks corresponding to metal stripes with a Gaussian function yields the full width at half maximum of 36 μm. This can be again explained by the fact that the contrast significantly increases when the metal provides a high-frequency short between the two electrodes of the tip. It is worth to note that the scan over the stripes reveals the full modulation depth as observed in the scans over a single metal edge. The curve marked by (d) shows a scan over a metal edge at a frequency of 80 GHz based on the continuous-wave experimental setup shown in Fig. 1(c).
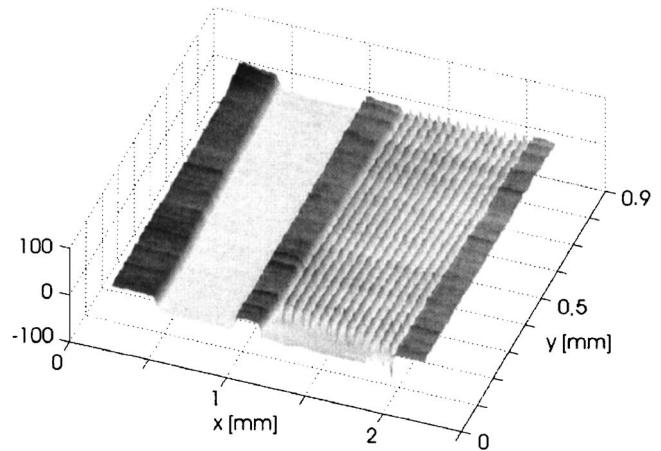
Again, the measured resolution of 17 μm indicates that its frequency dependence is rather weak, as expected due to the quasistatic nature of the electric field at the tip. It is worth to note that this value corresponds to 1/200 of the free space wavelength.

As an illustration of the imaging ability of our approach, Fig. 5 shows a two-dimensional scan taken at 80 GHz over a 1-mm-wide metal stripe and an array of 30-μm-wide stripes being separated by gaps of 30 μm.

IV. CONCLUSION

In summary, we have developed a promising technique for millimeter-wave and terahertz near-field imagings with a high potential to perform micrometer or submicrometer spatially resolved spectroscopy at terahertz frequencies. The resolution was proven to be much smaller than the wavelength. We hope that by employing refined fabrication techniques for our tips such as the focused ion-beam etching we will be soon able to achieve a resolution of 1 μm or below. Beyond its capability for terahertz near-field imaging and spectroscopy, the high electric field at the tip might make our approach suitable for ultrafast writing of (sub)micrometer-sized domains in ferroelectric films.

[1]*Sensing with Terahertz Radiation*, edited by D. Mittleman (Springer, Berlin, 2003).
[2]D. A. Crawley, C. Longbottom, B. D. Cole, C. M. Ciesla, D. Arnone, V. P. Wallace, and M. Pepper, Caries Res. **37**, 352 (2003).
[3]X.-C. Zhang, Philos. Trans. R. Soc. London, Ser. A **362**, 283 (2004).
[4]B. B. Hu and M. C. Nuss, Opt. Lett. **20**, 1716 (1995).
[5]J. Nishizawa, T. Sasaki, K. Suto, T. Yamada, T. Tanabe, T. Tanno, T. Sawai, and Y. Miura, Opt. Commun. **244**, 469 (2005).

[6]Q. Wu, T. D. Hewitt, and X.-C. Zhang, Appl. Phys. Lett. **69**, 1026 (1996).

[7]Z. Jiang and X.-C. Zhang, Opt. Lett. **23**, 1114 (1998).

[8]S. Wang and X.-C. Zhang, Appl. Phys. Lett. **82**, 1821 (2003).

[9]S. Hunsche, M. Koch, I. Brener, and M. Nuss, Opt. Commun. **150**, 22 (1998).

[10]Q. Chen, Z. Jiang, G. X. Xu, and X.-C. Zhang, Opt. Lett. **25**, 1122 (2000).

[11]N. van der Valk and P. Planken, Appl. Phys. Lett. **81**, 1558 (2002).

[12]H.-T. Chen, R. Kersting, and G. C. Cho, Appl. Phys. Lett. **83**, 3009 (2003).

[13]H.-T. Chen, S. Kraatz, G. C. Cho, and R. Kersting, Phys. Rev. Lett. **93**, 267401 (2004).

[14]A. Tselev, S. M. Anlage, H. N. Christen, R. L. Moreland, V. V. Talanov, and A. R. Schwartz, Rev. Sci. Instrum. **74**, 3167 (2003).

[15]M. Golosovsky and D. Davidov, Appl. Phys. Lett. **68**, 1579 (1996).

[16]M. Abu-Teir, M. Golosovsky, D. Davidov, A. Frenkel, and H. Goldberger, Rev. Sci. Instrum. **72**, 2073 (2001).

[17]S. Kirstein, Curr. Opin. Colloid Interface Sci. **4**, 256 (1999).

[18]M. De Serio, M. Zenobi, and V. Deckert, Trends Analyt. Chem. **22**, 70 (2003).

[19]A. Nahata, A. S. Weling, and T. F. Heinz, Appl. Phys. Lett. **69**, 2321 (1996).

[20]Computer Simulation Technology, http://www.cst.com.